DOI: 10.13009/EUCASS2017-512

Physics of SLD Impact and Solidification

Cameron Tropea⋆† *Markus Schremb and Ilia V. Roisman*
⋆*Institute of Fluid Mechanics and Aerodynamics, Technische Universität Darmstadt*
Alarich-Weiß-Straße 10, 64287 Darmstadt, Germany
ctropea@sla.tu-darmstadt.de
†Corresponding author

Abstract

The hydrodynamics and thermodynamics of supercooled large drops (SLD) impacting onto, and freezing on solid surfaces will be examined. Four distinctly different processes can be identified and models for each of these are introduced. A statistical model describes nucleation, which includes the influence of the impact hydrodynamics, as opposed to sessile drops. The subsequent solidification proceeds in three phases. An ice layer forms on the surface, rapidly spreading over the substrate. In the bulk, dendrites propagate at a slower speed, which is dependent on the degree of supercooling. Once the bulk has warmed up to zero degrees, due to the latent heat of solidification of the dendrites, the remaining fluid solidifies according to the one-phase Stefan problem and does so at an even slower rate than the dendrite growth. This process of drop impact, spreading, retraction, nucleation and solidification is illustrated and analysed using experimental results, theoretical descriptions and numerical simulations. This contribution summarizes the state of the art in describing SLD impact and solidification. It then concludes with an outlook about outstanding problems and indications of how these physical models can be incorporated into practical icing codes.

1. Introduction

Ice accretion represents a severe hazard in transportation systems such as aviation,[4] shipping[26,51] and road traffic,[46] but is also a well-known danger for power lines[9,10,47] and wind turbines. In many instances ice accretion results from the impact of water drops onto a surface at subfreezing temperatures. If the liquid is also supercooled, the freezing process becomes unstable and ice nucleation is followed by the fast propagation of a cloud of dendrites throughout the drop, during which the remaining liquid portion of the drop warms to the freezing temperature. This rather rapid propagation of dendrites is followed by a slower solidification of the remaining liquid, corresponding to the planar Stefan problem.[7,19] These four processes, nucleation followed by three phases of solidification, are pictured graphically in Fig. 1. Each process has its own characteristic time scale and specific physics; hence, individual models for each process must be identified and/or developed.

On a dry surface the spreading of the drop, i.e. the hydrodynamic behavior, is largely unaffected by the temperature of the substrate before nucleation occurs, exhibiting only minor dependencies related to the change of viscosity at low temperatures.[40] Thus, a large body of literature addressing the hydrodynamics of drop impact onto dry surfaces with no phase change is immediately applicable.[18,32,48,49] However, once nucleation occurs, the rapid propagation of dendrites inhibits further hydrodynamic spreading and/or receding. This 'mushy' state of the drop will exhibit different rheology, depending on the density of the dendritic growth; hence, the drop's deformation due to aerodynamic shear or the conditions for incipient motion will also be strongly affected. Therefore, the nucleation instant and the associated *freezing delay* is of utmost importance in defining the final iced area and is an essential ingredient into any physics based accretion model.

Solidification of sessile drops starts as a result of the nucleation of ice embryos when they exceed a critical size, corresponding to thermodynamic equilibrium. It is well established that nucleation is a spontaneous process dependent on temporal and spatial fluctuations of temperature and density of the liquid phase.[30] Since these fluctuations are molecular in nature, nucleation in sessile drops is a stochastic process. In many cases heterogeneous nucleation at the substrate surface dominates freezing onset of sessile drops on cold surfaces. While the spreading kinetics of a drop impacting onto a warm surface is well known, the effect of drop impact on the nucleation rate and therefore on the freezing delay are still not well understood. The influence of hydrodynamics on the nucleation rate is the subject of the following section 2.

DOI: 10.13009/EUCASS2017-512

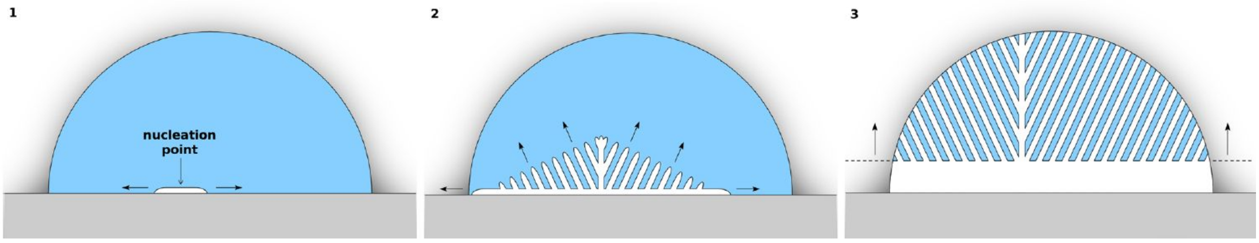

Figure 1: Three phases of solidification of a supercooled drop in the vicinity of a solid wall: (1) heterogeneous nucleation and spreading of a thin ice layer at the substrate, (2) dendritic freezing of the bulk liquid, (3) freezing of the remaining water at T_m. Note that the orientation of the dendrites in 2 and 3 is only schematic. Reprinted with permission.[39] Copyright 2017 American Chemical Society.

Following nucleation, the first phase of solidification pictured in Fig. 1 (1) is the tangential and rapid growth of an ice layer on the substrate. This will be discussed in section 3. The second phase of solidification, shown in Fig. 1 (2), begins as an instability of the ice layer growth and exhibits rapid dendritic growth throughout the entire drop. This dendritic growth and the subsequent and slower solidification of the bulk is the subject of section 4 (Fig. 1 (3)).

If the impact surface is already covered with ice, then the entire solidification process can be modified. Solidification occurs instantaneously upon impact and an ice layer begins forming immediately on the substrate without any observable *freezing delay*. This is the situation encountered once a first layer of ice has formed on the substrate and this will be discussed in section 5.

All of the above topics have been the focus of research at the Institute of Fluid Mechanics at the Technische Universität Darmstadt over the past years and the present article is a review of progress in this field. The contribution ends with an outlook about problems, which are still outstanding and about prospects for using the physics presented in this study in the framework of icing codes for simulating airframe icing.

A number of topics will not be addressed in the present contribution. The hydrodynamics of isothermal drop impact without phase change will not be reviewed, since this is well covered in previous review articles and books.[48,49] Similarly, the dislodging, deformation or shedding of sessile drops by aerodynamic shear under icing conditions will not be discussed, since these affects will be arrested once nucleation has commenced and dendrites have spread throughout the bulk liquid. The reader is referred to previous literature for more details about prediction of drop motion on a surface and its numerical treatment.[3,27,35,37] This latter topic is often associated with the three-phase contact angle, the contact angle hysteresis and its numerical treatment. Thus, many studies have investigated the influence of hydrophobic or superhydrophobic surfaces on incipient drop motion or shedding; however, once an ice layer forms, the contact angle changes dramatically and then the question of surface roughness replaces the issue of contact angle. This feature of substrates, i.e. the roughness of ice layers, and their influence on the hydrodynamics and thermodynamics of SLD impact is much less studied and has also been omitted from the present overview.

2. Nucleation and Freezing Delay

The random nature of nucleation suggests that a statistical model should be possible to formulate by observing nucleation over a large number of identical experiments. Such a model for heterogeneous nucleation has been developed, based on a large number of impact experiments using drops and substrates at temperatures between +17° C to -17° C. The experimental apparatus,[40] pictured schematically in Fig. 2, comprises a drop generation system, an enclosed impact plate chilled and held at a constant temperature, and a high-speed video camera operating at 2 500 frames/s with a spatial resolution of 45 µm/pixel.

A set of images in Fig. 3 shows the freezing process in a receding drop, appearing as an expansion of a dark, initially nearly circular region. Since the temperature of the substrate is well below the freezing temperature, the liquid in the near-wall region is below the freezing temperature as well. According to Roisman (2010),[33] the temperature at the contact surface between the liquid and the substrate is calculated as $-14.7°$ C. Therefore, the frozen region shown in Fig. 3 is a cloud of ice dendrites, typical for solidification of supercooled liquids.[19,41] The cloud is initiated by heterogeneous nucleation on the target substrate, since the temperatures are well above the homogeneous nucleation temperature of approximately $-40\,°$C.[15] The observed nucleation sites in the drops are distributed uniformly over the wetted area of the target. This result is in agreement with earlier observations of heterogeneous nucleation.[13] It should be noted that nucleation is not always observed, neither in the period of spreading nor receding. However, in many other cases the drop starts to freeze. In these cases the moment of nucleation and subsequent solidification determines

DOI: 10.13009/EUCASS2017-512

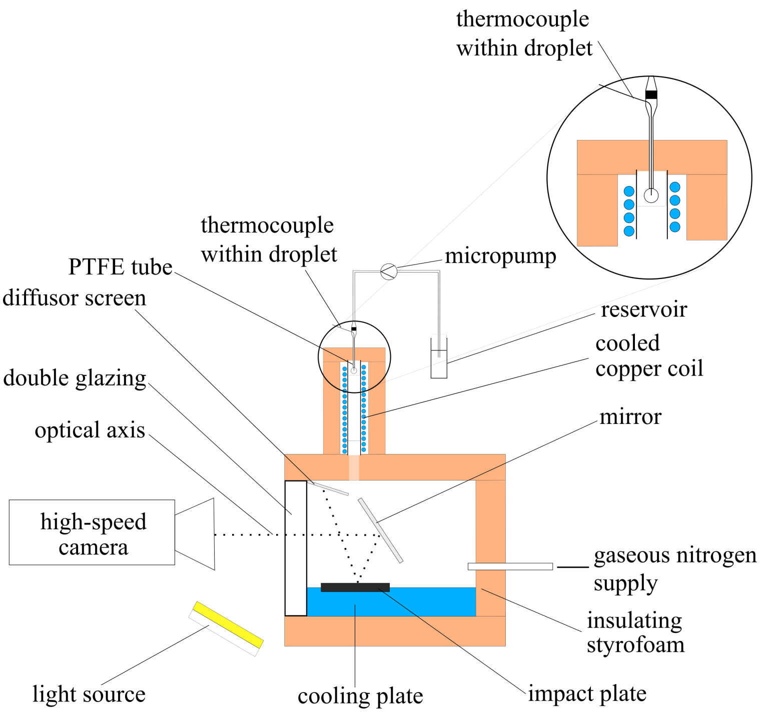

Figure 2: Schematic of the experimental setup. Reprinted with permission.[40] Copyright 2017 by the American Physical Society.

the residual shape of the drop; hence the conclusion: the hydrodynamics of drop impact determines the potential iced area and the thermodynamics determines the final iced area.

Nucleation is a random process which follows certain statistics, obtained by analysis of multiple experiments at the same operational conditions. In the following, a statistical model is formulated using the hypothesis that the probability of nucleation will scale with the wetted area and since the wetted area changes with time, this variation must be incorporated into the model. Denote by N_0 the total number of drop impact experiments. Each nucleation event in a drop at instant t reduces the number of drops remaining liquid at this time by one. The number of liquid drops therefore continuously reduces in time. Denote by $N_{\text{liq}}(t)$ the number of liquid drops, namely the number of drops whose freezing time is larger than t. An example of the ratio $N_{\text{liq}}(t)/N_0$ is shown in Fig. 4 for the case of inclined impact of water drops at room temperature onto a cold surface. The evolution of the number of liquid drops is not a smooth function since it is determined by the average nucleation rate and by the wetted area, which changes in time due to the drop spreading and receding.

Denote $J_{\text{s}}(t)$ as an instantaneous rate of nucleation per unit area. In the case of drop impact it can include a constant rate associated with the self-nucleation at the liquid-solid interface and the rate associated with the embryos flux from the bulk liquid. Since the nucleation rate does not depend on the position, the average number of active nucleation sites on an element of the wetted surface area, ΔA, is $\Delta\lambda = \int_{t_{\text{w}}}^{t} J_{\text{s}} \mathrm{d}t\, \Delta A$, where t_w is the instant when the given area element is wetted by the spreading drop for the first time. Therefore, the total average number of the nucleation sites per drop can be estimated as

$$\lambda(t) = \int_0^{A_c(t)} \left(\int_{t_{\text{w}}(A_c)}^{t} J_{\text{s}} \mathrm{d}t \right) \mathrm{d}A, \tag{1}$$

where $A_{\text{c}}(t)$ is the wetted surface area at time t. In equation (1) it is assumed that the potential nucleation site in a definite location at the substrate disappears during dewetting. Otherwise these sites would collect in the vicinity of the contact line. However, no increase of nucleation near the contact line has been observed.

For long times after impact, $t \gg t_{\text{w}}$, the time of drop spreading can be neglected in comparison to the total time of nucleation and the expression for the average number of nucleation sites reduces to

$$\lambda(t) \approx A_c(t) \int_0^{t} J_{\text{s}} \mathrm{d}t. \tag{2}$$

Since the process of nucleation is completely random, the statistics of the number of active nucleation sites follows the Poisson distribution.[11] This means that the probability that a single drop contains exactly n nucleation sites

DOI: 10.13009/EUCASS2017-512

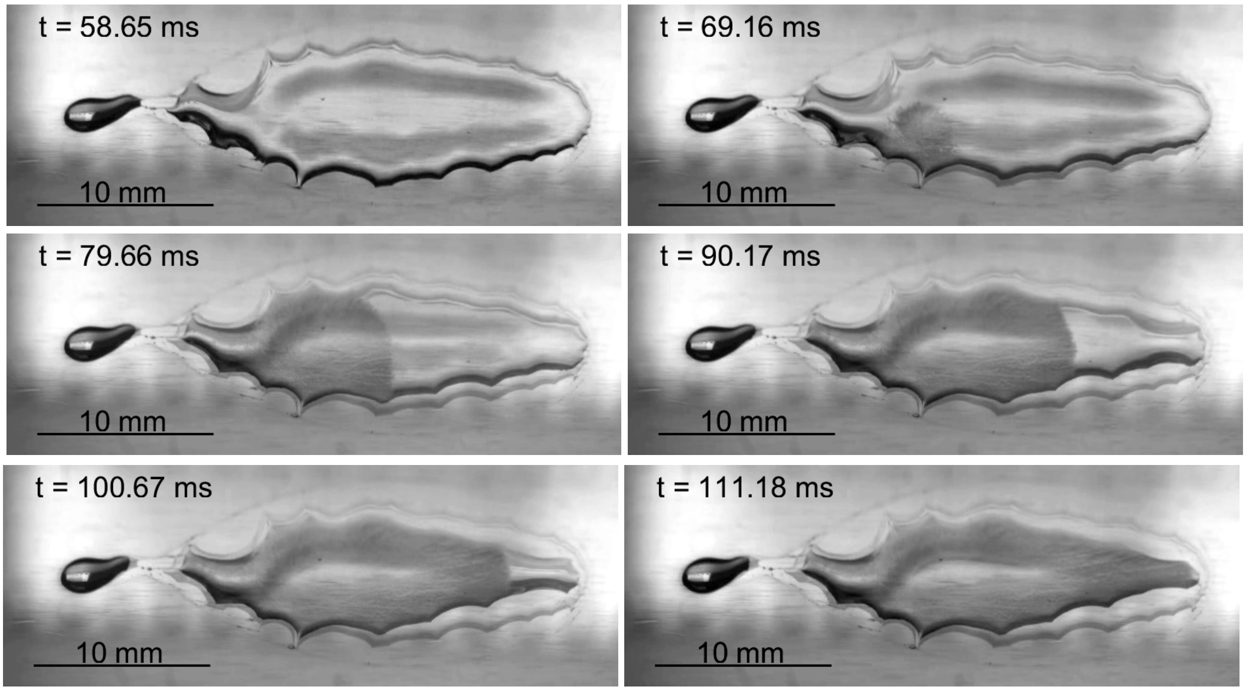

Figure 3: Exemplary time sequence of the propagation of a freezing front of dendrites within a receding drop after oblique impact onto polished aluminum. The drop is initially at 14.3° C and the substrate at −17.0° C. To illustrate the further receding during freezing, every frame is superposed with the frame at t = 58.65 ms as reference. Reprinted with permission.[40] Copyright 2017 by the American Physical Society.

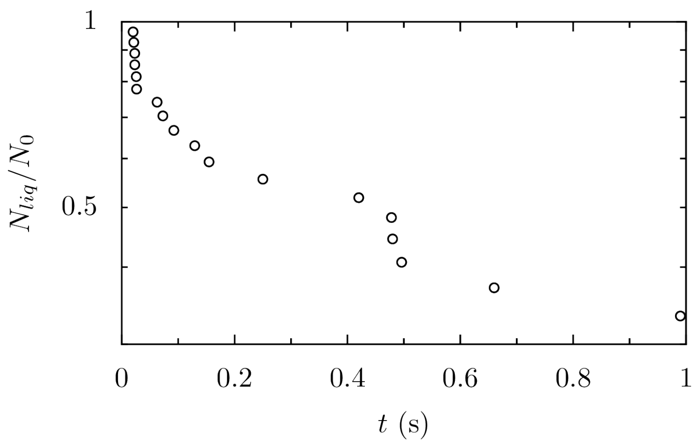

Figure 4: Relative number of liquid drops, N_{liq}/N_0, as a function of time for a water drop at 14.3° C impacting onto a cold, polished, aluminum substrate at −17.0° C. Drop initial diameter is 3.09 mm and the impact velocity is 4.09 m/s. The impact angle is 30°. Reprinted with permission.[40] Copyright 2017 by the American Physical Society.

DOI: 10.13009/EUCASS2017-512

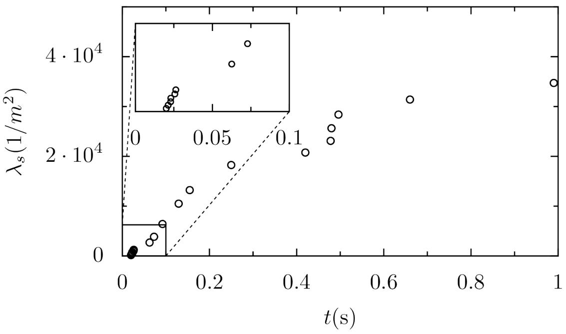

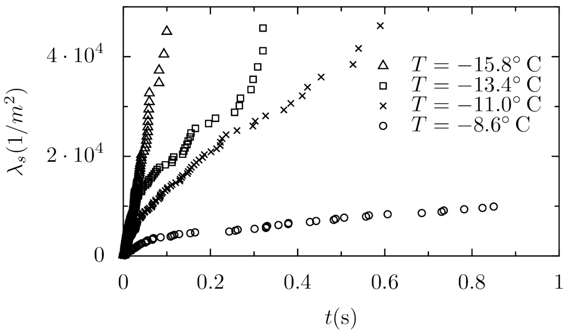

Figure 5: Average number of nucleation sites per unit area as a function of time. Left graph: water drops at 14.3° C impacting onto a cold, polished, aluminum substrate at −17.0° C. Drop diameter is 3.09 mm and the impact velocity is 4.09 m/s. The impact angle is 30°. The contact temperature $T_c = -14.7°$ C is estimated using theory.[33] Right graph: supercooled water drops impacting onto a cold, sandblasted, glass substrate. The temperatures of the substrate and of the drop are the same. Drop diameter is 3.2 mm and the impact velocity is 2.2 m/s. The impact angle is 90°. Reprinted with permission.[40] Copyright 2017 by the American Physical Society.

is

$$p(n;\lambda) = \exp[-\lambda]\frac{\lambda^n}{n!}. \tag{3}$$

For any time t the probability $p(0;\lambda) = \exp[-\lambda]$ of the absence of nucleation sites can be estimated experimentally as a relative number of the liquid drops, whose freezing time is larger than t.

Consider statistics of N_0 initially liquid drops impacting onto a cold substrate. The nucleation time of each drop is denoted t_n and can be determined from the experiments. The number of all the liquid drops $N_\mathrm{liq}(t)$, whose nucleation time is larger than t, continuously reduces in time. The above analysis yields the following remote asymptotic relation between the relative number of liquid drops and the nucleation rate

$$\frac{1}{A_c(t)} \quad \ln \quad \frac{N_0}{N_\mathrm{liq}(t)} = \lambda_s(t), \tag{4}$$

$$\lambda_s \quad \equiv \quad \int_0^t J_s \mathrm{d}t, \tag{5}$$

for times much longer than the time of drop spreading, $t \gg t_\mathrm{spreading}$, where $\lambda_s(t)$ is the average number of the nucleation sites per unit area.

The values of $\lambda_s(t)$ estimated from the experiments using the approximate expression (4) are shown in Fig. 5 for the impact of warm drops (left graph) and for impacts of supercooled drops (right graph) with various initial temperatures. In all the cases, we observe a time-dependent nucleation rate. For the case of supercooled drops, the nucleation rate is relatively high during the first 35 milliseconds after drop impact and is smaller for longer times. Moreover, a clear time lag for nucleation of approximately 20 milliseconds is observed for oblique impact of warm drops (see the insert in Fig. 5a).

Several physical mechanisms can be considered as influencing factors on the nucleation rate. Which mechanisms are most relevant and dominating can be identified by comparing their respective time scales to the time scales for rate changes observed in the experiments. Using this approach the pressure pulse associated with the drop impact can be eliminated, as can the flow in the drop.[40] However, the effect of air bubbles and bubble cavitation on the intensification of nucleation or on the reduction of the nucleation temperature is well known.[5,14] Air bubbles may be entrapped within the rough surface during drop impact, especially during drop spreading over the rough surface.[2] In this case, the size of the bubbles is comparable with the roughness of the surface. For polished aluminium it is approximately 1 µm. Such bubbles are almost invisible with a microscope. While for earlier times, nucleation is supported by the presence of gas bubbles on the substrate surface, for longer times pure heterogeneous nucleation on the wetted substrate dominates the process. It should be noted that for small wall bubbles the lifetime can be much longer, which can lead to a non-constant nucleation rate even at longer times after drop impact.[25]

In order to more explicitly confirm this hypothesis on the influence of bubble formation on the nucleation rate of impacting drops, impact experiments were performed with drops of different gas content. The gas content in the drops was varied between the saturation gas content at a pressure of 1 atm and at a pressure of 0.1 atm. In the experiments both the drop and the wall temperature is −11° C. In the case of non-degassed water, many more air bubbles in the form of small black spots on the wetted surface area can be observed than for the case of degassed water. This effect can be

DOI: 10.13009/EUCASS2017-512

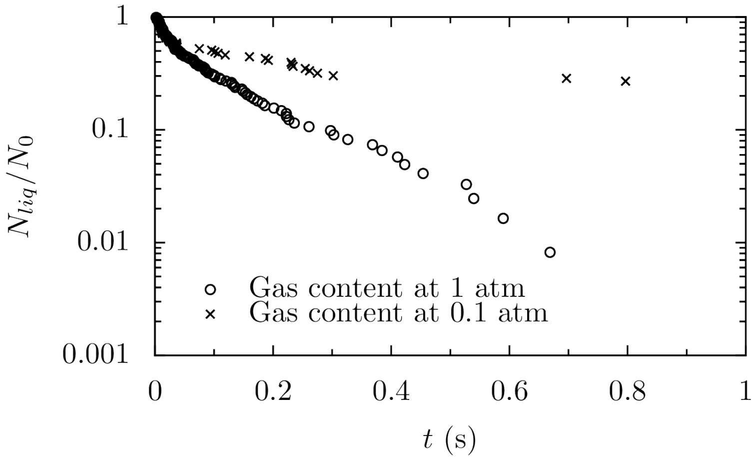

Figure 6: Relative number of liquid drops, N_{liq}/N_0, as a function of time for water drops with different gas contents at $-11.0°$ C impacting onto a cold, sandblasted, glass substrate. The temperatures of the substrate and of the drop are the same. Drop diameter is 3.2 mm and the impact velocity is 2.2 m/s. The impact angle is 90°. Reprinted with permission.[40] Copyright 2017 by the American Physical Society.

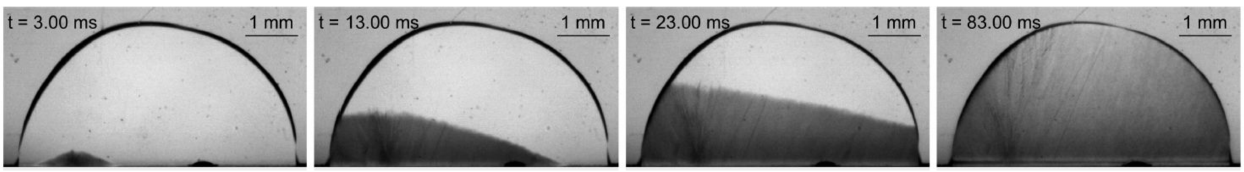

Figure 7: Dendritic freezing of a water drop at $-15.6°$ C in the Hele−Shaw cell. Reprinted with permission.[39] Copyright 2017 American Chemical Society.

explained by the faster dissolving of the bubbles in the degassed liquid. The observed relative number of liquid drops N_{liq}/N_0 is shown in Fig. 6. The nucleation rate for degassed drops is much smaller, thus confirming the hypothesis concerning the influence of entrapped air bubbles.

In summary, for inclined drop impact of water drops at room temperature, the surface temperature influences the hydrodynamics of drop impact.[40] For low substrate temperatures, the contact area and contact time between the liquid and the substrate are increased in consequence of varying liquid properties. Nucleation is heterogeneous on the substrate surface and therefore, the surface temperature implicitly influences the drop freezing rate by increasing the contact area and contact time. Based on repeated impact experiments for constant conditions, a statistical model has been developed to derive the rate of heterogeneous nucleation. The model incorporates the variation of the wetted surface area. It has been shown that the nucleation rate during and after impact depends on time and is the highest in a short phase after impact. Air bubbles at the impact surface which are generated during drop impact serve as additional nucleation sites and therefore, increase the nucleation rate. Experiments with degassed water drops exhibit a clear dependence of the nucleation rate on the liquid gas content. For a lower gas content of the liquid, the nucleation rate decreases. Air bubbles at the impact surface dissolve faster in the surrounding liquid, decreasing the time of enhanced nucleation. For supercooled drops, the average number of nucleation sites per unit area increases significantly.

3. Spreading of a thin Ice Layer on the Substrate

Having examined the freezing delay through nucleation in the previous section, the present section is devoted to the subsequent process of solidification of a liquid on a solid substrate. This process can be divided into three phases, pictured schematically in Fig. 1 and using photographs taken from a Hele-Shaw apparatus in Fig. 7. The first stage is the spreading of a thin ice layer at the substrate, the second is the dendritic freezing of the bulk liquid and the third is the freezing of the remaining liquid. In this section the first phase will be discussed; the latter stages follow in subsequent sections, but are briefly summarized below.

The Hele-Shaw apparatus used to visualize the solidification in Fig. 7 was introduced by Schremb and Tropea (2017)[41] and consists of two side walls made of acrylic glass and an exchangeable spacer at the base, made of different

DOI: 10.13009/EUCASS2017-512

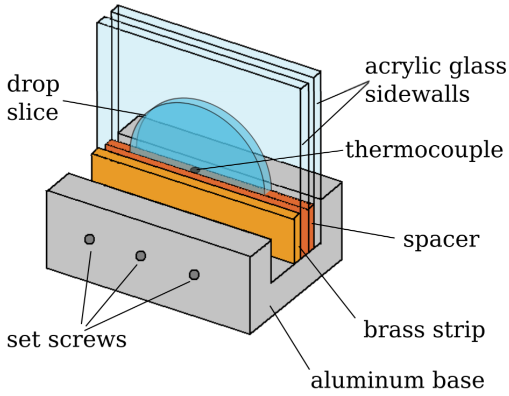

Figure 8: Schematic of the Hele-Shaw cell with an inserted drop. Reprinted with permission.[39] Copyright 2017 American Chemical Society.

materials, which provides a constant distance between the side walls. A water drop is trapped between the side walls and is in direct contact with the spacer material, as depicted in Fig. 8. The freezing process is observed with a high-speed video camera, operated at a frame rate of 2000 frames/s with a resolution of 512x256 pixels. The temperature of the drop is measured with a thermocouple immersed into the substrate or in the drop. At the beginning of each experiment, the Hele-Shaw cell and drop, both at room temperature, are placed onto a cooling plate, which is cooled down at a moderate cooling rate of approximately 0.2 K/s, resulting in a simultaneous cooldown of the substrate and the drop. The temperature at the moment of freezing is obtained as the lowest value before the steep rise of the temperature signal, corresponding to freezing at the substrate surface.

In the first phase, heterogeneous nucleation at the wall is followed by the tangential growth of a thin ice layer spreading over the substrate/water interface with a constant speed, which depends on supercooling. For supercooling up to $\Delta T = 7$ K, the velocity of the initial ice layer strongly depends on the material properties of the solid substrate.[21] However, Kong and Liu (2015)[21] and Schremb and Tropea (2017)[40] suggested that the solidification velocity is only weakly influenced by the substrate material for larger supercooling. For large supercooling, the surface of the initial ice layer becomes unstable at a certain position behind the tip of the ice layer, resulting in the growth of single dendrites or a front of numerous dendrites into the bulk liquid, as shown in Fig. 7. The supercooling threshold for unstable growth was found as $\Delta T = 2.6$ K in Kong and Liu (2015)[21] and as $\Delta T = 4.7$ K in Schremb and Tropea (2017).[40] For supercooling below this threshold, only planar growth of the thin ice layer has been observed. The higher the supercooling, the closer to the ice layer tip is the position of the first instability of the ice layer surface. This instability will be discussed in section 4.

In the second phase, the growth of dendrites arising from the layer instability is observed. While single dendrites are observed for smaller supercooling, the dendrite density increases with increasing supercooling, resulting in a dense front of dendrites for large supercooling. At the end of the second phase, only a portion of the initially supercooled drop is frozen and a lattice of dendritic ice fills the entire drop, as shown in the last image of Fig. 7. The latent heat released during solidification has warmed up the water/ice mixture to thermodynamic equilibrium at the melting temperature.

A further removal of heat results in stable freezing of the remaining water, constituting the third phase. The stable freezing front in this phase moves in the opposite direction of the applied heat flux. This freezing phase starts during the ongoing dendritic freezing of the liquid and can be observed in the last two images of Fig. 7 as a thin layer of changed brightness near the substrate surface.

Fig. 9 shows the experimentally measured ice layer velocities for varying degrees of supercooling and substrate materials. For comparison, experimental data of Shibkov *et al.* (2003)[44] for the velocity of a single dendrite growing freely in supercooled water is also shown. In contrast to the solidification at the metallic surfaces, in the case of the acrylic glass substrate, no explicit growth of a thin ice layer has been observed. Therefore, the movement of the intersection point of the dendritic front and the substrate surface has been assumed to be comparable to the ice layer propagation. The horizontal velocity of this point is shown in Fig. 9. The solidification velocity on the acrylic glass substrate is very similar to the velocity of a single dendrite. Thus, the acrylic glass substrate acts as an adiabatic wall and does not thermally influence the solidification process in the near wall region. However, as already observed by Kong and Liu (2015)[21] and Schremb and Tropea (2017),[40] the ice layer velocity is drastically enhanced by the presence of a metallic substrate in comparison to the velocity of a single dendrite. Furthermore, a strong dependence of the ice layer velocity on the substrate material has been observed for supercooling up to $\Delta T = 7$ K by Kong and Liu (2015).[21] However, as shown in Fig. 9, in the case of metallic substrates, the substrate material only weakly influences the ice layer propagation velocity for larger supercooling. These results underline the importance of capturing the conjugate heat transfer problem associated with the substrate in any model or prediction. This issue has recently been addressed in terms of appropriate computational modelling.[38]

DOI: 10.13009/EUCASS2017-512

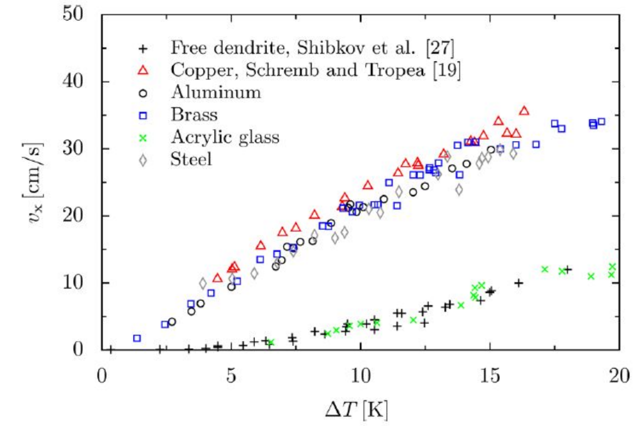

Figure 9: Ice layer velocity as a function of supercooling for varying substrate materials. Experimental data of Shibkov *et al.* (2003)[44] for the velocity of a single dendrite growing freely in supercooled water is also shown. Reprinted with permission.[39] Copyright 2017 American Chemical Society.

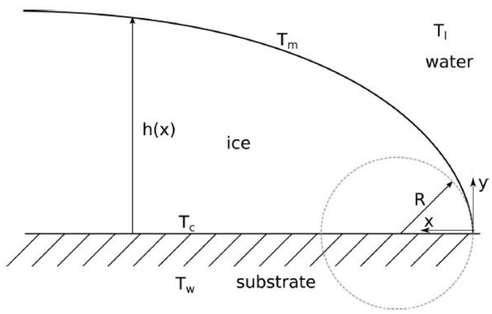

Figure 10: Cross-sectional view of the modeled ice layer. Reprinted with permission.[39] Copyright 2017 American Chemical Society.

The propagation of the initial ice layer, the first phase, has been theoretically modeled.[39] On the basis of the analytic solution of the two-phase Stefan problem, the model explicitly incorporates heat conduction in the supercooled liquid and in the growing ice layer. Heat conduction in the solid wall, which is the origin of the increased velocity in the case of the metallic substrates, is implicitly accounted for by the estimation of the surface temperature below the ice layer. It is calculated using the equation for the contact temperature between two semi-infinite slabs of different temperature suddenly brought into contact. The only free parameter in the theoretical model is a length scale characterizing the tip radius of the propagating ice layer (R). A cross-sectional view of the modeled ice layer is shown in Figure 10, showing also the tip radius. The tip radius has been found by a least-squares fit of the theoretical model to the experimental data, and it has been shown that this parameter does not depend on the substrate material and is furthermore constant for the entire diffusion limited growth regime. The reasons for the constancy of the tip radius are not clear so far and therefore deserve further examination. However, the experimental data in the range of supercooling $\Delta T \leq 10$ K is well described by the semi-empirical model. For higher supercooling, kinetic effects, which are not accounted for in the model, become important. These effects involve a decreasing speed of molecular attachment at the ice/water interface, which results in smaller velocities than predicted with the thermal model employed. These effects are discussed in more detail in section 4.

Figure 11 shows a direct comparison of the experimental and theoretical data for the ice layer velocity calculated with a constant tip radius of $R = 352$ nm. The solid line represents perfect agreement between the calculated and measured values. Even with the constraint of a substrate-independent tip radius, the theoretical model remains in very good agreement with the experimental data in the diffusion-limited growth regime. For layer velocities larger than 0.2 m/s, an increasing deviation between the theoretical and experimental data is observable; the model overpredicts the layer velocity. Figure 11 also shows a comparison for the data obtained on the acrylic glass substrate. The experimental data for acrylic glass are not used for the calculation of the tip radius R, and no distinct ice layer growth is observable on acrylic glass. Nevertheless, the agreement between the modeled growth velocity and the experimental values is very good.

4. Two Phases of Freezing in the Bulk

The final two stages of solidification, depicted graphically in in Figure 1, consist of an initial rapid, recalescent stage of crystallization (dendritic growth) followed by a final slower, quasi-isothermal stage (stable planar solidification). Although these two stages have been identified experimentally, e.g. Jung *et al.* (2012) ,[19] the modelling of these stages was unclear until recently. The initial computational model used to capture this heat diffusion problem[6,31] has been

DOI: 10.13009/EUCASS2017-512

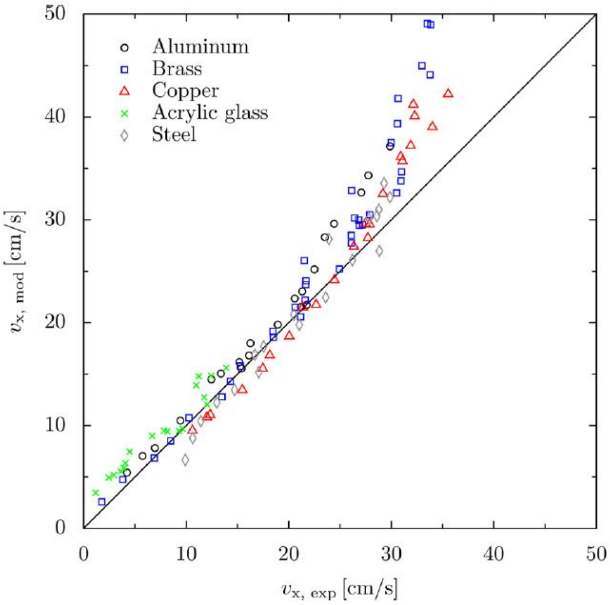

Figure 11: Comparison of the theoretically modeled and experimentally measured layer velocity for all substrate materials. A constant tip radius of $R = 352$ nm was used for the calculation. Reprinted with permission.[39] Copyright 2017 American Chemical Society.

modified for high-fidelity discretization of the thermal-energy equation and with regard to the normal-to-the-interface temperature gradient determination. For supercooling ΔT above $\approx$ 5K, the model exhibits deviation from available experimental data. This is attributed to kinetic effects influencing the growth of individual dendrites. In this section the refined model will be briefly introduced and its results compared to experimental data.

The solid-liquid interface, representing the phase-transition region where solid and liquid coexist, is characterized by a planar shape for most pure materials under ordinary freezing conditions, implying a constant interface temperature T_m, Fig. 12 I . During the crystallization of supercooled water the interface between the solid and the liquid phase becomes unstable to small interface curvature perturbations. The supercooling acts towards an interface destabilization with the solidification rate depending on the degree of the initial supercooling, which drives this process. On the contrary, the interfacial energy tends to stabilize the interface, damping small perturbations back in line with the Gibbs-Thomson relation, Fig. 12 II. The balance between the stabilizing and destabilizing effects can be analyzed by the classical approach to morphological instability introduced by Mullins and Sekerka[28,29] in the context of directional solidification, Fig. 12 III. The analysis of the morphological instability yields the cutoff wavelength representing the largest possible wavelength for a stable interface:

$$\lambda_c \approx \sqrt{\frac{2\alpha T_m \sigma c_v}{v_{n,0} L_v^2}} \approx \sqrt{\delta_d \delta_c}, \tag{6}$$

where α is the thermal diffusivity, $L_v = L\rho$ and $v_{n,0}$ represents the characteristic velocity of the system. $\delta_d = 2\alpha / v_{n,0}$ and $\delta_c = T_m \sigma c_v / L_v^2$ represent the thermal diffusion and the capillary length scale, respectively. The wavelength of the fastest growing mode, λ_f, is defined as[12]

$$\lambda_f = \sqrt{3}\lambda_c. \tag{7}$$

At this wavelength, interfacial perturbations should grow fastest into the supercooled liquid.

Assuming that the thermal diffusivity, α, and the volumetric heat capacity, c_v, are constant, the cutoff wavelength depends directly on $v_{n,0}$. If the value of the interface velocity increases, the largest possible wavelength for a stable interface decreases. Thus, the cutoff wavelength gets smaller at higher supercooling for the liquid phase subjected to the condition which implies a constant temperature gradient in the solid. This theoretical statement is verified by experiments.

Ivantsov[16] derived an analytical solution for the steady-state tip velocity and the tip radius of growing dendrites, under the following assumption: first, the kinetics is instantaneous, $k_{\text{kin}}^{-1} = 0$, second, the surface energy is zero, $\sigma = 0$, and third, the crystal tip has a parabolic structure. This theory considers a single needle growing into an infinite half-space of supercooled liquid. The Péclet number, Pe, is used to establish a correlation between the tip velocity, v_t,

DOI: 10.13009/EUCASS2017-512

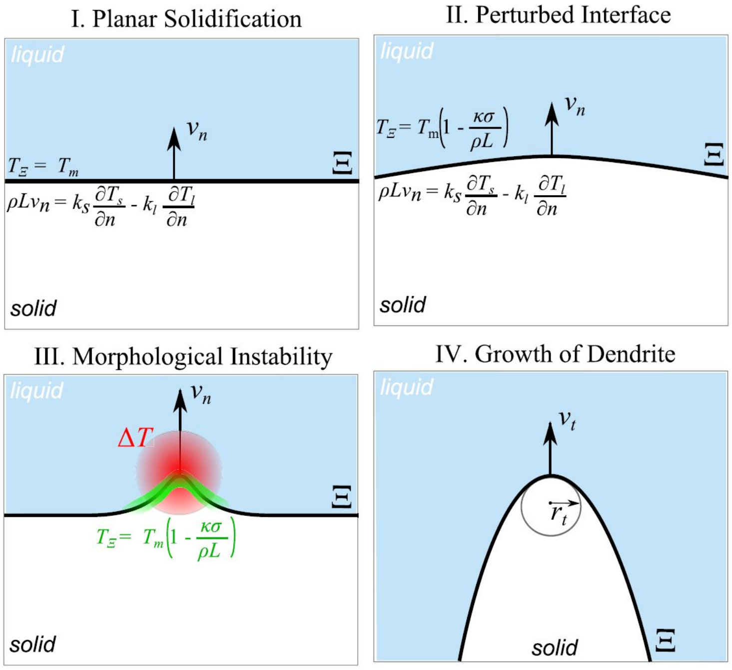

Figure 12: Sequence of events, from planar freezing front to the growth of needle-like dendrites.[7]

and the tip radius, r_t:

$$\mathrm{Pe} = \frac{v_t r_t}{2\alpha}. \tag{8}$$

There is a unique Péclet number valid for the entire range of dimensionless supercooling, $\Delta = \Delta T/(L/c_p)$, obtained by solving the Ivantsov function:

$$\Delta = \mathrm{Pe}_0 \exp^{\mathrm{Pe}_0} E_1(\mathrm{Pe}_0). \tag{9}$$

The solution of this function represents a continuous family of parabolas/paraboloids for a given initial dimensionless supercooling Δ. One of the first important hypothetical principles regarding the tip-shape selection was the Marginal Stability Theory (MST) introduced by Langer and Müller-Krumbhaar[22–24] in their work on *Universal Law of Crystal Growth*. They analyzed the stable steady-state of the Ivantsov paraboloidal dendrite introducing the interfacial energy effect as a linearized perturbation function and found that the Ivantsov's continuum family of solutions may be divided into a stable and an unstable region. When interfacial energy, σ, is present and kinetic supercooling is neglected, a new dimensionless parameter can be defined, representing the so-called controlling parameter for the operating point of the needle:

$$\epsilon = \frac{T_m \sigma c_v 2\alpha}{L_v^2 v_n r_{t^2}} = \frac{\delta_c \delta_d}{r_{t^2}} = \frac{\lambda_c}{2\pi r_t}. \tag{10}$$

The selected dendrite corresponds to the point of marginal stability; hence the emerging tip radius, r_t, corresponds to the cutoff wavelength, Eq. (6). Eq. (10) provides an additional relation between the tip growth velocity and the tip radius. The first relation is provided in terms of the Peclét number, Eq. (8). On the basis of the MST, a unique tip growth velocity as a single valued function of the supercooling can be calculated. However, for larger supercooling, the theory overpredicts the growth rate of dendrites, as pictured in Fig. 13 (MST - solid black line).

Shibkov et al. (2005)[43] pointed out that considering the effects pertinent to the kinetics-limited dendrite growth is of importance in the higher supercooling range ($\Delta T > 5$). Unfortunately, there are few studies in the literature about how such a phenomenon could be quantified in the framework of a mathematical model. The starting point of the present modelling activity is the work of Davis (2001)[8] who suggested the velocity of the solid-liquid interface at high supercooling to be approximated by a linear function of a fraction of the total undercooling originating from molecular kinetics, ΔT_{kin}.

$$v_n = k_{kin}(T_m - T_\Xi) = k_{kin}\Delta T_{kin}, \tag{11}$$

where k_{kin} represents the kinetic coefficient. Accordingly, the effect of the kinetic undercooling at the interface can be modeled as follows:

$$T_\Xi = T_m - k_{kin}^{-1} v_n. \tag{12}$$

DOI: 10.13009/EUCASS2017-512

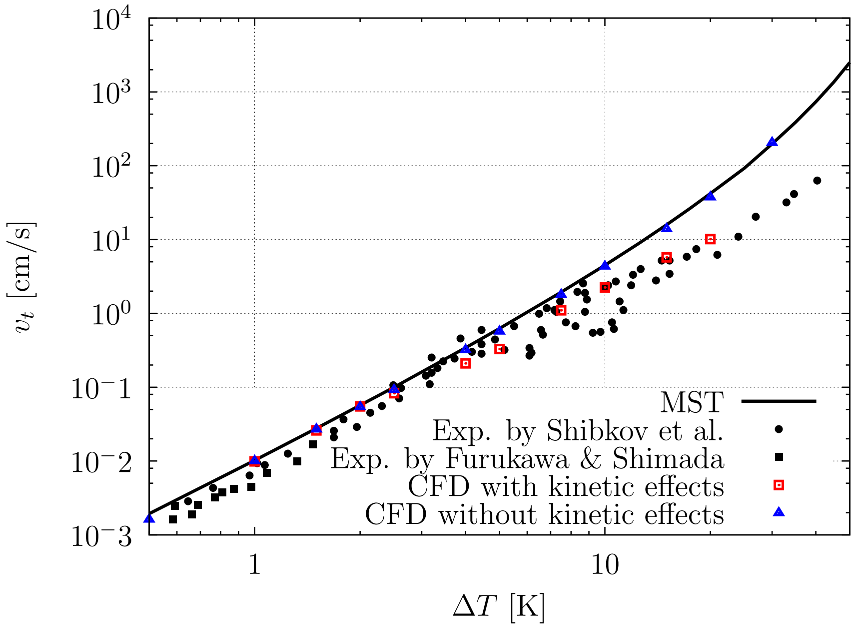

Figure 13: Steady state tip velocity, v_t, dependence on initial supercooling ΔT for $\lambda_s/\lambda_f = 1$: computational vs. MST-theoretical and experimental results; the results obtained by present empirical model accounting for kinetic undercooling at the solid-liquid interface exhibit good agreement with reference experiments over the entire range of initial supercooling.[7]

This approximation is valid for pure substances with low latent heat of crystallization such as pure metals and water. The intensity of a coefficient accounting for the kinetic effects originating from the molecular rearrangement at the interface from liquid state to a solid state (denoted as kinetic coefficient k_{kin}) is, to date, not well defined in the scientific literature. In the following, an empirical model for the kinetic coefficient is outlined. It represents a revised version of the model derived in Criscione *et al.*[6] In order to quantify the model term mimicking the kinetics-limited growth the theoretical and experimental results displayed in Fig. 13 are comparatively analyzed. First of all, it is assumed that the steady-state dendrite tip velocity determined experimentally in Shibkov *et al.*(2005),[45] $v_{n,exp}$, is directly proportional to

$$v_{n,exp} \propto \Delta T_T. \tag{13}$$

with ΔT_T representing the total undercooling (consisting of viscous and kinetic fractions, ΔT_v and ΔT_{kin} respectively) at the solid-liquid interface, which is defined as

$$\Delta T_T = \Delta T_v + \Delta T_{kin}. \tag{14}$$

In the analytical MST solution, the viscous undercooling is accounted for. In order to account for the kinetic undercooling, the ratio of the theoretical steady-state velocity (related to the viscous undercooling only) to the experimentally determined one (influenced in addition also by the kinetic undercooling), $|\Delta v_n| = v_{MST}/v_{n,exp}$, is computed assuming its proportionality to the ratio of the viscous (capillary) undercooling to the total one

$$\Delta T_T = \frac{\Delta T_v}{|\Delta v_n|}. \tag{15}$$

Inserting it into Eq. (14) and adopting a linear function for the kinetic undercooling, Eq. (11), the following expression for the kinetic coefficient is obtained

$$k_{kin} = \frac{|\Delta v_n| v_{MST} L\rho}{(1 - |\Delta v_n|)\kappa\sigma T_m}. \tag{16}$$

The preliminary results obtained at high supercooling degrees by accounting for the kinetic undercooling in the present computational model exhibit good agreement with the experimental data. The only limitation when using Eq. (16) is that the kinetic coefficient is directly dependent on the theoretical steady-state velocity; hence, on the initial supercooling degree. In order to find a coefficient value valid for all supercooling degrees considered, the relation between the

DOI: 10.13009/EUCASS2017-512

kinetic coefficient and the theoretical steady-state velocity is introduced by applying the following relation:

$$k_{\mathrm{kin}} = \xi \left(v_{\mathrm{MST}}\right)^{\frac{2}{3}}, \tag{17}$$

The value of the coefficient ξ representing a pre-exponential factor, determined, i.e. calibrated by relevance to the reference experiment by Shibkov et al. (2003)[44] (see Fig. 13), amounts finally $(\pi/11)^{2/3}$. Accordingly, the coefficient ξ represents a dimensional quantity whose unit corresponds to $m^{1/3}/\left(s^{1/3}K\right)$. Under consideration of Eq. (11), the kinetic undercooling can be formulated as follows:

$$\Delta T_{\mathrm{kin}} = \frac{v_{\mathrm{n}}}{k_{\mathrm{kin}}}. \tag{18}$$

Assuming that the solid-liquid interface velocity, v_{n}, corresponds to the theoretical value v_{MST} obtained by neglecting the kinetic effects, the kinetic undercooling can be redefined resulting in following equation:

$$\Delta T_{\mathrm{kin}} = \frac{\left(v_{\mathrm{MST}}\right)^{\frac{1}{3}}}{\xi}. \tag{19}$$

Herewith, the appropriate quantification of the kinetic undercooling influence on the dendrite growth in the high supercooling range is provided. After accounting for the kinetic effects by considering the present approach the computational results at high supercooling degrees follow closely the experimental results, Fig. 13. Further details of the numerical procedure used can be found in Criscione *et al.* (2015) .[7]

This second stage of solidification is followed by the third stage, as schematically depicted in Fig. 1. The difference between the second and the third stage is characterised by the direction of the heat flux. During the second stage, the latent heat of solidification is mainly added to the liquid due to high supercooling. After the second stage the initial supercooling is exhausted. The drop temperature rises to the crystallization temperature. The ratio of the sensible heat, $c_{\mathrm{v}}\Delta T$, to the latent heat, L, reveals that only a portion (e.g. 18.8% for $\Delta T = 15$ K) of the drop volume is solidified after the first stage of crystallization.

At the beginning of the third stage, the temperature of the drop remains constant at the melting temperature, T_{m}. Due to an appropriately colder substrate in the experiments, the heat is now removed via heat conduction into the substrate. Fig. 14 illustrates the mechanism of the freezing pertinent to the third stage. The heat is conducted from the solid phase (having higher heat conductivity) to the substrate. After the second stage the solidified water becomes colder and consequently cools down the water between the dendritic needles. Thus, the water begins to freeze upwards from the solid cold boundary representing the substrate. The relevant solidification front velocity is considerably lower compared to the freezing velocity characteristic of the second stage. The third stage of freezing can be mathematically described as a one-dimensional freezing, starting from a cold boundary. To verify this theory, a suitable one-dimensional simulation setup is configured, Fig. 14. The initial temperature in both the solid and liquid phases is $T_{\mathrm{s}} = T_{\mathrm{l}} = 273.15$ K. The lower domain boundary at $T_{\mathrm{sub}} = 258.15$ K represents the cooling substrate. An adiabatic condition at the upper domain boundary is prescribed and the symmetry-plane condition was adopted at the right and left domain sides. At this point, it should be mentioned that the freezing process is also influenced by the thermal diffusivity of the substrate affecting the freezing front velocity. Experiments by Jung *et al.* (2012)[19] confirm this behavior. In the present work, the influence of the thermal diffusivity is neglected; a constant temperature of the substrate is assumed when simulating the third stage of freezing.

In the experiments of Jung *et al.* ,[20] the volume of the supercooled water drop is 5 µl, i.e. assuming a perfectly spherical shape of the drop the corresponding diameter would be equal to 2.11 mm. The duration of the thrid crystallization stage is approx. 20 s. Computations with different grid resolutions show, first, that the results converge unambiguously to the analytical solution at lower grid resolutions[31] and second, that the height of the growing ice layer after 20 s reaches the value of 1.997 mm, Fig. 15. The gain in volume and, consequently, in velocity of the solidification front during the phase change is negligibly small (only ca. 3% of the front velocity), being as such represented also in the present computations. Therefore, we can conclude that the governing equations describing the solidification mechanism resembling a heat-diffusion-based solidification model can account for both freezing stages: second dendritic stage and third planar stage solidification.

Based on the present computational results, the different mechanisms underlying the latter two solidification stages can be explained as follows: in the second stage the initial planar solidification front becomes morphologically unstable due to a high degree of supercooling. Small bumps/instabilities evolving at the interface propagate further into the liquid, causing a relevant steepening of the temperature gradient at the liquid side of the interface, contributing decisively to its rapid growth. During this transition process the small bumps at the solid-liquid interface develop into crystals of different shapes. At higher degrees of supercooling, $\Delta T \geq 5$ K, the instabilities grow into a dense array of dendritic needles. A small fraction of the drop freezes rapidly, not more than enough to raise up the temperature, i.e. until the thermal energy rate originating from supercooling is exhausted. The crystallization front can be modeled as

DOI: 10.13009/EUCASS2017-512

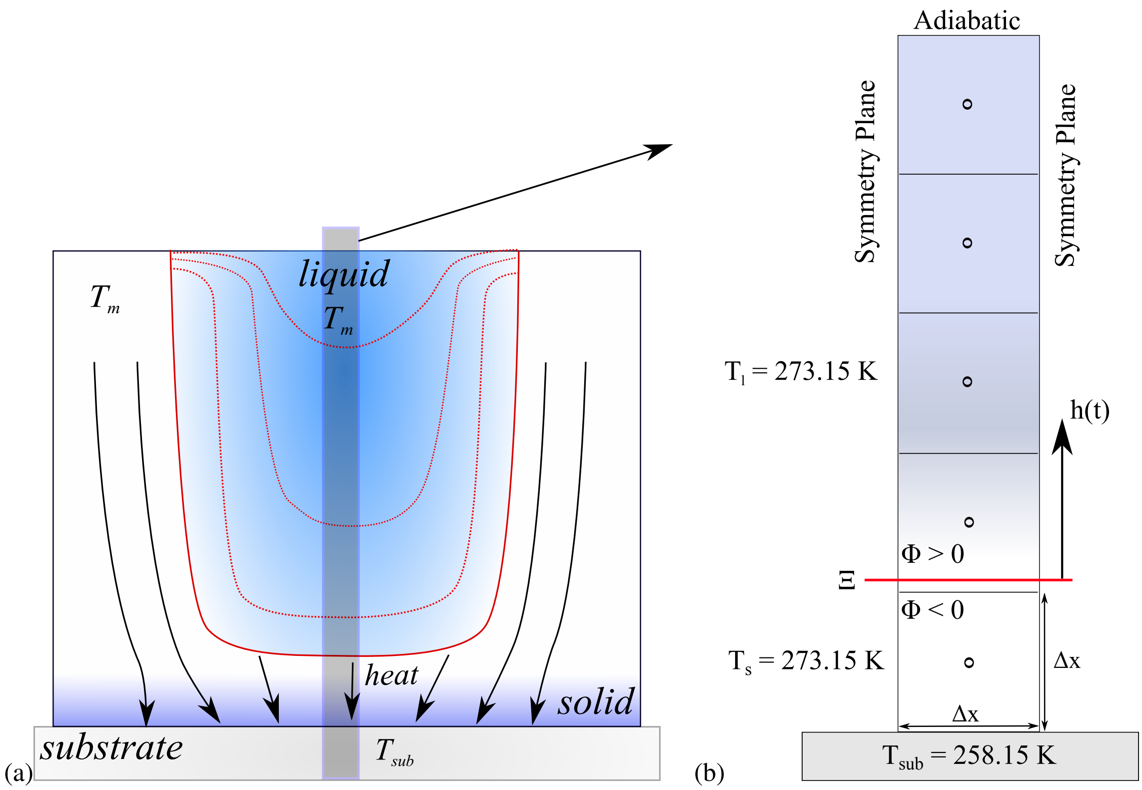

Figure 14: (a) A sketch of the freezing mechanism in the second stage: heat from the solid phase, at $T_m = 273.15$ K, is conducted to the cold substrate. Water between needle-like dendrites starts to freeze: red dotted lines visualize the possible time evolution of the solidification front. (b) A two-dimensional simulation setup, referring to freezing mechanism in the second stage, is depicted from the sketch; initial temperature in both the solid and liquid phase values $T_s = T_l = 273.15$ K. The lower boundary condition at the substrate, $T_{sub} = 258.15$ K, represents the cooling substrate. Adiabatic upper boundary condition and symmetry-plane condition at the right and left side close the setup. The mesh resolution is defined by Δx, whereas $h(t)$ describes one-dimensional growing solid/ice layer from the bottom/substrate to the top as a function of time.

growing needle-like dendrites influenced by kinetic effects.
In the third stage, the drop loses heat by evaporation and conduction. Within a sessile drop, the cold substrate cools the water between the needles and, accordingly, the ice layer front grows up planar from the cold boundary. The velocity of the solidification front is considerably lower than the freezing velocity in the second stage. The third stage can be mathematically described as a one-dimensional solidification process.

5. Freezing of a Supercooled Water Drop on an Ice Substrate

The previous results all pertain to a drop freezing on a dry, clean substrate; however in practice, drops often impact and solidify on an iced surface. The impact and solidification of water drops at room temperature onto an ice surface has been investigated by Jin *et al.* (2017).[17] However, to the authors' knowledge the impact of single supercooled water drops onto a smooth ice surface, resulting in immediate solidification of the impacting supercooled water drop, has never been investigated before. The following results relate to the influence of a varying substrate and drop temperature on the ice layer thickness after a single drop impact at subfreezing conditions.

To investigate these phenomena, the experimental apparatus pictured in Figure 2 is used, but the target is now an aluminum cooling plate, held at a constant temperature, with a cylindrical aluminum impact target placed on top. The diameter of the iced impact surface is comparable to the drop diameter and therefore, it is smaller than the maximum spread of the impacting drop.

In contrast to other materials, only ice causes immediate freezing when it is brought into contact with supercooled water. In this case an ice/water interface already exists and no further energy is required to form it. Water molecules may immediately attach to the existing interface to pass into the thermodynamically preferable stable state. Since nucleation denotes the formation of a first solid embryo from the liquid phase, this mechanism is strictly speaking

DOI: 10.13009/EUCASS2017-512

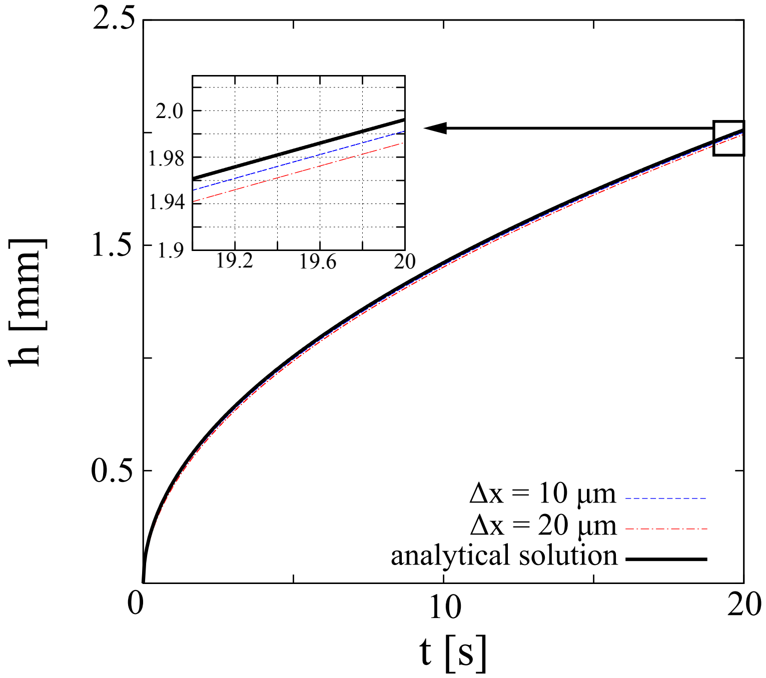

Figure 15: Growing ice layer plotted against time; simulations converge to the analytical solution of the one-dimensional planar solidification.[1] After 20 s the ice layer reaches an height of 1.997 mm; in experiments[19] the water drop has a volume of 5 μl, assuming a spherical shape it leads to a diameter of 2.11 mm. The gain in volume during the phase change is not accounted in computations.

not nucleation and should rather be called seeding. While the ice nucleating ability of catalysts consisting of other materials depends on the liquid temperature and the form or size of the catalyst particles, the ability of ice to trigger solidification of supercooled water is independent of the liquid temperature. This causes the main difference between an impact onto a dry solid substrate and an impact onto an ice surface. In the case of drops at room temperature and supercooled water drops impacting onto a dry solid substrate, stochastic nucleation results in strongly varying freezing delay times after impact, as discussed above. Fluid flow during drop impact and solidification do not start at the same time and the varying moment of nucleation drastically influences the final outcome of such a drop impact event.

Nucleation does not necessarily take place at the impact position; however, for simplicity the radial spreading of both the spreading initial ice layer and the drop are assumed axisymmetric in the schematic illustration of Figure 16. As shown in this figure, the radial growth of the ice layer of radius $r_{ice}(t)$ is independent of the radial expansion of the spreading drop, $r_w(t)$. While the spreading dynamics of the drop depends on the impact parameters and the material properties of the liquid, which may significantly vary with temperature, the spreading of the ice layer mainly depends on temperature. The initial temperature of the drop and the substrate, and the thermal properties of both, determine the contact temperature at the wetted surface. This temperature is the characteristic temperature for heterogeneous nucleation and freezing at the substrate's surface. However, besides their influence on the contact temperature, the thermal properties of the substrate also influence the solidification velocity parallel to the wall by determining the conduction of latent heat into the substrate. Therefore, the tangential expansion of the initial ice layer along the solid substrate only depends on the supercooling of the impinging drop, and the initial temperature and thermal properties of the substrate. Thus, the solidification process is independent of the radial spreading of the impacting drop.

Liquid is ejected from the edges of the impact surface during spreading and the formation of a pronounced rim around the center of impact, which would hinder the observation of the processes in the center of drop impact, is suppressed. Therefore, the lamella thinning and the resulting ice layer thickness above the point of impact can be observed undisturbed.

Figure 17 exemplarily shows the impact process of a supercooled water drop at -14.0°C onto the ice impact target at -14.0°C. At time $t = 0$ the drop makes contact with the ice impact surface and begins to spread over the surface. Simultaneously, freezing of the supercooled liquid starts at the solid-liquid interface. The moving contact line reaches the edge of the ice surface at $t \approx 0.36$ ms and for $t > 0.36$ ms, the spreading liquid is ejected from the edge of the ice surface. It forms a free expanding lamella around the impact target while the lamella continues thinning above the impact target. Since the drop diameter is comparable to the diameter of the ice impact target, the lamella is not

DOI: 10.13009/EUCASS2017-512

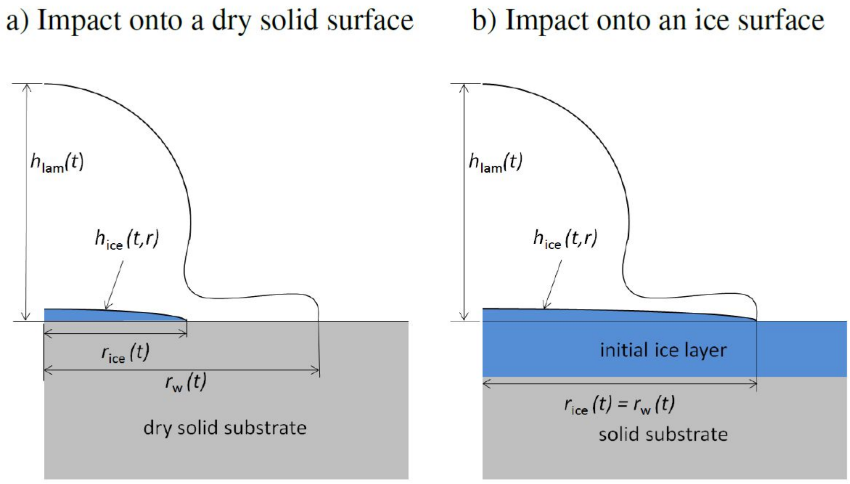

Figure 16: Two-dimensional schematic of the solidification during impact of a supercooled drop a) onto a dry solid surface and b) onto an ice surface.[42]

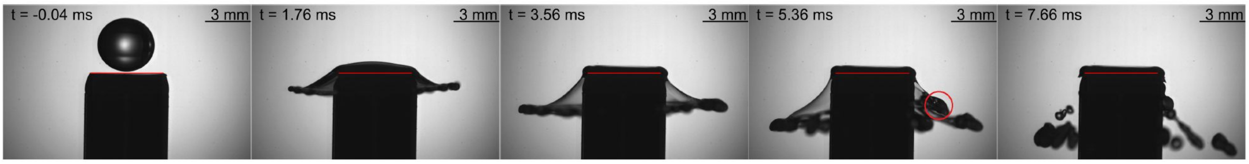

Figure 17: Dynamics during impact of a water drop supercooled to $-14.0°C$ onto a small ice impact target at $-14.0°C$. The red horizontal lines indicate the surface of the ice impact surface. The red circle in the fourth frame marks a position of freezing in the free liquid lamella, causing rupturing of the thin liquid film.[42]

ejected horizontally but under a certain angle to the horizontal.[36]

The experimental results will now be discussed in terms of the lamella thinning and the ice layer growth. For Re≫25 and We≫2.5, inertia dominates the flow in the spreading lamella of an impacting drop and Roisman *et al.*[34] found a relation for the temporal evolution of the lamella thickness. At the beginning of the impact the rear part of the impacting drop moves similar to a rigid body and accordingly, the lamella thickness at the center of impact, $r = 0$ can be described in the initial impact period $t < 0.4 d_d/v_d$ as

$$h_{lam}\,(t, r = 0) = d_d - v_d t. \tag{20}$$

For $t > 0.7 d_d/v_d$ the expressions for the radial velocity of the lamella and its thickness are obtained from the inviscid solution[34,50] for the flow in the spreading drop

$$u_r = r\left(\frac{d_d}{v_d}\tau + t\right)^{-1}, \quad h_{lam}\,(t, r = 0) = \eta d_d \left(\tau + \frac{v_d}{d_d} t\right)^{-2}, \tag{21}$$

where d_d and v_d are the diameter and velocity of the impacting drop, $\eta \approx 0.39$ and $\tau \approx 0.25$ are dimensionless constants.[34] This expression later was modified to account for the expansion of the viscous boundary layer expanded near the wall.[32]

Figure 18 shows the temporal evolution of the lamella thickness for different temperatures. For comparison, the evolution of the lamella thickness calculated with Eqs. 20 and 21 is also shown in Fig. 18. For the impact conditions of the present study, these relations are valid in the ranges $t < 0.618$ ms and $t > 1.082$ ms, respectively, which is indicated by means of the dashed vertical lines in the figure. Up to $t \approx 3.5$ ms, the theoretical predictions 20 and 21 are in good agreement with the experimental data.

At some instant (2.5 - 4 milliseconds, depending on the initial temperature) the measured lamella thickness starts to significantly deviate from the theoretical curve. At larger times the flow in the lamella is increasingly damped. The residual film thickness depends on the initial temperature.

For long times after impact, when the thicknesses of the lamella and of the viscous boundary layer are of the same order, the remote asymptotic solution (21) is no longer valid since viscosity damps the velocity of the spreading

DOI: 10.13009/EUCASS2017-512

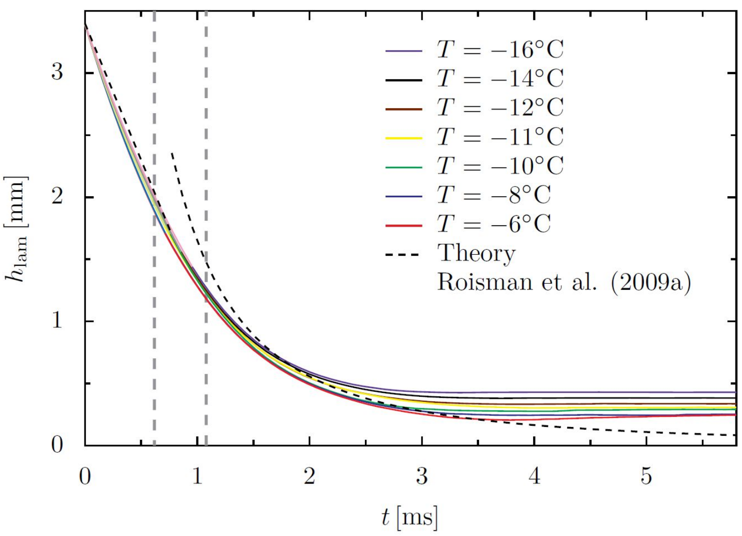

Figure 18: Temporal evolution of the lamella thickness depending on the initial drop and surface temperature in comparison to theoretical predictions according to Eqs. (20) and (21).[42]

lamella. The residual film thickness[32] in the absence of solidification is

$$h_{\text{visc}} \approx 0.79 d_d \text{Re}^{-2/5}, \tag{22}$$

where $Re \equiv d_d v_d/\nu$ is the Reynolds number. In these experiments the expression for h_{visc} predicts the residual film thickness of approximately 100 micrometers, which is much smaller than the observed residual thicknesses. This fact indicates the dominant influence of solidification on the flow in the spreading lamella at the later stages of drop spreading.

Since the liquid is supercooled, the solidification process proceeds as outlined in the previous section. The influence of the dendrite cloud on the lamella flow can be estimated assuming that the dendrites in the cloud are strong enough not to be damaged by the flow in the lamella. This assumption is supported by the fact that the yield stress of ice ($Y \sim 10$ MPa) is much higher than the stresses associated with drop impact ($p \sim \rho v_d^2 \sim 10^{-3} - 10^{-1}$ MPa). The upper bound for the lamella thickness in this situation can be evaluated assuming that the velocity of the liquid flow in the porous dendrite/liquid cloud is much smaller than the flow in the lamella above the cloud. Moreover, a viscous boundary layer is developed at the interface of the expanding dendrite cloud $z = \upsilon_f t$, where υ_f is the velocity of the dendrite growth. The velocity field in the lamella which satisfies the continuity equation and the boundary conditions at $z = \upsilon_f t$ is assumed in the form of a remote asymptotic solution

$$u_r = f(y)\frac{r}{t}, \quad u_z = \frac{g(y)}{t} \tag{23}$$

$$f(0) = 0, \quad g(0) = 0, \quad f(\infty) \to 1 \tag{24}$$

where $y \equiv z - \upsilon_f t$. It takes into account the fact that τ is small at large times. The continuity and momentum balance equations for the flow in the lamella in the coordinate system moving with the dendrite front yield the following asymptotic equations, valid for long times after impact when the boundary layer can be considered quasi-steady

$$g'(y) + 2f(y) = 0, \quad \upsilon_f f'(y) + \nu f''(y) = 0. \tag{25}$$

The solution of this equation is obtained in the form

$$f = 1 - \exp\left[-\frac{\upsilon_f y}{\nu}\right], \quad g = -2y + \frac{2\nu}{\upsilon_f}\left(1 - \exp\left[-\frac{\upsilon_f y}{\nu}\right]\right). \tag{26}$$

Therefore, the axial velocity outside the boundary layer is

$$u_z(z,t) \approx \frac{2}{t}\left(\frac{\nu}{\upsilon_f} - z\right) + 2\upsilon_f. \tag{27}$$

DOI: 10.13009/EUCASS2017-512

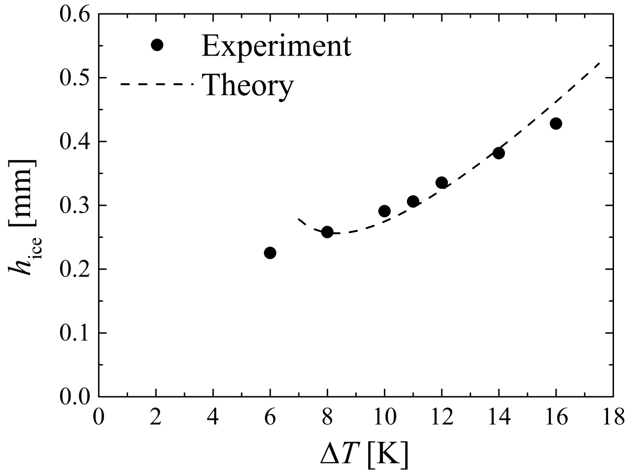

Figure 19: Final ice thicknesses $h_{\rm ice}$ for various initial temperatures in comparison with the theoretical predictions (30), valid for $\nu v_d d_d^{-1} \upsilon_{\rm f}^{-2} \ll 1$.

The evolution of the lamella thickness can be now evaluated integrating the ordinary differential equation $u_z(h_{lam}, t) = \dot{h}_{lam}$. The expression for the evolution of the lamella thickness, derived with the help of (27)

$$h_{lam}\,(t, r = 0) = \eta \frac{d_d^3}{t^2 v_d^2} + \frac{2\upsilon_{\rm f} t}{3} + \frac{\nu}{\upsilon_{\rm f}}, \tag{28}$$

is valid for large times.

The residual ice thickness $h_{\rm ice}$, associated with the instant t^* when the dendrites' height is equal to the lamella thickness is estimated as

$$t^* \approx d_d \upsilon_{\rm f}^{-1/3} v_d^{-2/3}, \tag{29}$$

$$h_{\rm ice} \approx d_d \upsilon_{\rm f}^{2/3} v_d^{-2/3} + \frac{\nu}{\upsilon_{\rm f}}, \quad \text{if} \quad \frac{\nu v_d}{d_d \upsilon_{\rm f}^2} \ll 1. \tag{30}$$

Expression (30) is valid only for high values of supercooling, ΔT, and thus for high enough values of the dendrite velocity $\upsilon_{\rm f}$, which satisfies the condition $\nu v_d d_d^{-1} \upsilon_{\rm f}^{-2} \ll 1$.

A comparison of the theoretical estimation of the ice layer thickness (30) with the measured data is shown in Fig. 19. The dependence of the dendrite cloud velocity on the initial temperature of the liquid is obtained by interpolation of the existing experimental data.[44] The agreement is rather good. However, for smaller supercooling, for which $\nu v_d d_d^{-1} \upsilon_{\rm f}^{-2} \gg 1$, the prediction, as expected, deviates from the experimental data. In this range of parameters both the expansion of the viscous boundary and the expansion of the dendrite cloud influence the flow in the lamella. This regime requires more accurate and more complicated modeling. As a lower bound, the viscous residual film thickness defined in Eq. (22) can be used for supercooled temperatures close to the melting point. Good agreement between the theory and experiment for high supercooling indicates that the main physical phenomena influencing the solidification process of a spreading supercooled drop are taken into account with this analysis.

In summary, the most important difference between the impact of a supercooled water drop onto a dry solid surface and onto an ice surface is the instant when freezing begins: while nucleation is stochastic in the case of an impact onto a dry solid surface, solidification starts simultaneously with the impact in the case of drop impact onto ice. This important difference allows to reproducibly investigate mutual influences between fluid flow and solidification during drop impact. The influence of the growing ice layer on the flow in the lamella becomes more significant for lower temperatures.

6. Open Questions and Modelling Prospects

To develop an overall model of ice accretion several important questions still have to be answered and several physical problems still have to be solved.

DOI: 10.13009/EUCASS2017-512

- *Aerodynamic shear flow on single drop impact hydrodynamics and on spray impact.* There is still no reliable model on the effect of the shearing gas flow on the splashing threshold, size and initial velocity of the secondary drops and the ratio of the deposited/splashed mass. A large number of tests is required to develop such models, since the number of influencing parameters is relatively high. However, there is now clear knowledge about which of these parameters is dominant for which conditions.

- *The effect of aerodynamic shear flow on all stages of solidification.* Model development for a *shear driven film flow* on a solid substrate is a rather challenging problem since it involves also unknown rheology of the dendrite/liquid water regions. The model involves an accurate determination of the aerodynamic forces driving the flow. These forces include not only the viscous shear stresses but also the pressure gradients in the air flow. The problem includes description of the incipient motion of *drops or rivulets*, their motion on different surfaces, transformation of the flow regimes, shedding and atomization. This problem has to be addressed by research groups familiar with such investigations, for instance those involved in air-blast atomization, vehicle water management, etc.

- *Instability of the shear driven film flow with solidification.* Such instabilities lead to the emergence of feathers or other ice shape patterns. The model must be able to predict the typical conditions for such instabilities and characteristic geometrical parameters. Since these instabilities are highly three-dimensional, complex and expensive direct numerical simulations are required for an accurate description of these phenomena and their analysis.

- *An accretion model* has to be developed, which is complementary and compatible to existing industrial computational tools. This model has to account not only for the drop deposition efficiency, but also for the flow of the liquid on the substrate and on the ice layer, which leads to the mass transport along the solid substrate and leads to the redistribution of the solid ice material. It is not immediately clear how to "teach" these codes how to describe various flow instabilities.

- *Computational codes* are required which are able to accurately predict the shear stresses and heat fluxes in the air and in the substrates, accounting for the substrate surface conditions, like ice layer roughness and porosity, formation of a liquid layer, etc.

- *Development of passive and active ice prevention systems.* One widely investigated concepts for icing prevention is in the use of superhydrophobic substrates, which can potentially help to shed the impacting drops, thus reducing the rate of ice accretion. Different coating materials have been fabricated and studied for reduction of the ice adhesion forces. Another possible direction, shown in this study, is in the use of non-conducting substrates, which also reduces the ice growth rate.

7. Acknowledgments

The authors gratefully acknowledge financial support from the Deutsche Forschungsgemeinschaft within the Collaborative Research Center SFB-TRR 75 (TP-C3). Furthermore, they acknowledge the substantial contributions of many doctoral students and colleagues over the past years, in particular Dr.-Ing. Edin Berberović, Dr.-Ing. A. Criscione and Prof. Suad Jakirlić.

References

[1] V. I. Alexiades, D. G. Wilson, and A. D. Solomon. Macroscopic global modeling of binary alloy solidification processes. *Quarterly of Applied Mathematics*, 43(2):143–158, 1985.

[2] S. G. Bankoff. Entrapment of gas in the spreading of a liquid over a rough surface. *AIChE Journal*, 4(1):24–26, 1958.

[3] S. Basu, K. Nandakumar, and J. H. Masliyah. A model for detachment of a partially wetting drop from a solid surface by shear flow. *Journal of Colloid and Interface science*, 190(1):253–257, 1997.

[4] T. Cebeci and F. Kafyeke. Aircraft icing. *Annu. Rev. Fluid Mech.*, 35(1):11–21, 2003.

[5] R. Chow, R. Blindt, R. Chivers, and M. Povey. A study on the primary and secondary nucleation of ice by power ultrasound. *Ultrasonics*, 43(4):227–230, 2005.

DOI: 10.13009/EUCASS2017-512

[6] A. Criscione, D. Kintea, Ž. Tuković, S. Jakirlić, I. Roisman, and C. Tropea. Crystallization of supercooled water: A level-set-based modeling of the dendrite tip velocity. *International Journal of Heat and Mass Transfer*, 66:830–837, 2013.

[7] A. Criscione, I. V. Roisman, S. Jakirlić, and C. Tropea. Towards modelling of initial and final stages of supercooled water solidification. *International Journal of Thermal Sciences*, 92:150–161, 2015.

[8] S. H. Davis. *Theory of Solidification*. Cambridge University Press, 2001.

[9] M. Farzaneh, editor. *Atmospheric Icing of Power Networks*. Springer Science & Business Media, 2008.

[10] M. Farzaneh and O. T. Melo. Properties and effect of freezing rain and winter fog on outline insulators. *Cold Reg. Sci. Tech.*, 19(1):33–46, 1990.

[11] W. Feller. *An Introduction to Probability Theory and its Applications*, volume I. Wiley, New York, 3rd edition, 1968.

[12] C. Godreche. *Solids far from Equilibrium*, volume 1. Cambridge University Press, 1991.

[13] C. Gurganus, A. B. Kostinski, and R. A. Shaw. Fast imaging of freezing drops: No preference for nucleation at the contact line. *The Journal of Physical Chemistry Letters*, 2(12):1449–1454, 2011.

[14] A. F. Heneghan and A. D. J. Haymet. Liquid-to-crystal heterogeneous nucleation: Bubble accelerated nucleation of pure supercooled water. *Chemical Physics Letters*, 368(1-2):177–182, 2003.

[15] P. V. Hobbs. *Ice Physics*. Oxford University Press, 2010.

[16] G. Ivantsov. Temperature field around spherical, cylindrical, and needle-shaped crystals which grow in supercooled melt. *Doklady Akademii Nauk SSSR*, 58:567–569, 1947.

[17] Z. Jin, H. Zhang, and Z. Yang. Experimental investigation of the impact and freezing processes of a water droplet on an ice surface. *International Journal of Heat and Mass Transfer*, 109:716–724, 2017.

[18] C. Josserand and S. T. Thoroddsen. Drop impact on a solid surface. *Annu. Rev. Fluid Mech.*, 48:365–391, 2016.

[19] S. Jung, M. K. Tiwari, N. V. Doan, and D. Poulikakos. Mechanism of supercooled droplet freezing on surfaces. *Nature communications*, 3:615, 2012.

[20] S. Jung, M. K. Tiwari, and D. Poulikakos. Frost halos from supercooled water droplets. *Proceedings of the National Academy of Sciences*, 109(40):16073–16078, 2012.

[21] W. Kong and H. Liu. A theory on the icing evolution of supercooled water near solid substrate. *Int. J. Heat Mass Transf.*, 91:1217–1236, 2015.

[22] J. S. Langer and R. F. Müller-Krumbhaar. Theory of dendritic growth–I. Elements of a stability analysis. *Acta Metallurgica*, 26:1681–1687, 1978.

[23] J. S. Langer and R. F. Müller-Krumbhaar. Theory of dendritic growth–II. Instabilities in the limit of vanishing surface tension. *Acta Metallurgica*, 26:1689–1695, 1978.

[24] J. S. Langer and R. F. Müller-Krumbhaar. Theory of dendritic growth–III. Effects of surface tension. *Acta Metallurgica*, 26:1697–1708, 1978.

[25] D. Lohse and X. Zhang. Surface nanobubbles and nanodroplets. *Reviews of Modern Physics*, 87(3):981, 2015.

[26] L. Makkonen. Salinity and growth rate of ice formed by sea spray. *Cold Reg. Sci. Tech.*, 14(2):163–171, 1987.

[27] D. K. Mandal, A. Criscione, C. Tropea, and A. Amirfazli. Shedding of water drops from a surface under icing conditions. *Langmuir*, 31(34):9340–9347, 2015.

[28] W. W. Mullins and R. Sekerka. Stability of a planar interface during solidification of a dilute binary alloy. *Journal of Applied Physics*, 35(2):444–451, 1964.

[29] W. W. Mullins and R. F. Sekerka. Morphological stability of a particle growing by diffusion or heat flow. *Journal of Applied Physics*, 34(2):323–329, 1963.

DOI: 10.13009/EUCASS2017-512

[30] H. R. Pruppacher and J. D. Klett. *Microphysics of Clouds and Precipitation*. Springer, 2 edition, 1997.

[31] P. Rauschenberger, A. Criscione, K. Eisenschmidt, D. Kintea, S. Jakirlić, Ž. Tuković, I. V. Roisman, B. Weigand, and C. Tropea. Comparative assessment of Volume-of-Fluid and Level-Set methods by relevance to dendritic ice growth in supercooled water. *Computers & fluids*, 79:44–52, 2013.

[32] I. V. Roisman. Inertia dominated drop collisions. II. An analytical solution of the navier–stokes equations for a spreading viscous film. *Phys. Fluids*, 21(5):052104, 2009.

[33] I. V. Roisman. Fast forced liquid film spreading on a substrate: flow, heat transfer and phase transition. *J. Fluid Mech.*, 656:189–204, 2010.

[34] I. V. Roisman, E. Berberović, and C. Tropea. Inertia dominated drop collisions. I. On the universal flow in the lamella. *Physics of fluids*, 21(5):052103, 2009.

[35] I. V. Roisman, A. Criscione, C. Tropea, D. K. Mandal, and A. Amirfazli. Dislodging a sessile drop by a high-Reynolds-number shear flow at subfreezing temperatures. *Physical Review E*, 92(2):023007, 2015.

[36] A. Rozhkov, B. Prunet-Foch, and M. Vignes-Adler. Impact of water drops on small targets. *Physics of Fluids*, 14(10):3485–3501, 2002.

[37] A. D. Schleizer and R. T. Bonnecaze. Displacement of a two-dimensional immiscible droplet adhering to a wall in shear and pressure-driven flows. *Journal of Fluid Mechanics*, 383:29–54, 1999.

[38] M. Schremb, S. Borchert, E. Berberovic, S. Jakirlic, I. V. Roisman, and C. Tropea. Computational modelling of flow and conjugate heat transfer of a drop impacting onto a cold wall. *International Journal of Heat and Mass Transfer*, 109:971–980, 2017.

[39] M. Schremb, J. M. Campbell, H. K. Christenson, and C. Tropea. Ice layer spreading along a solid substrate during solidification of supercooled water: Experiments and modeling. *Langmuir*, 2017.

[40] M. Schremb, I. V. Roisman, and C. Tropea. Transient effects in ice nucleation of a water drop impacting onto a cold substrate. *Physical Review E*, 95(2):022805, 2017.

[41] M. Schremb and C. Tropea. Solidification of supercooled water in the vicinity of a solid wall. *Phys. Rev. E*, 94(5):052804, 2016.

[42] M. Schremb, T. Webert, and C. Tropea. Experimental investigation of supercooled water drops impacting onto a smooth ice surface. interaction of fluid flow and phase change. In *Proceedings of the 9th World Conference on Experimental Heat Transfer, Fluid Mechanics and Thermodynamics*, Iguazu Falls, Brazil, 2017.

[43] A. Shibkov, M. A. Zheltov, A. A. Korolev, and A. A. Leonov. Kinetic phase diagram of fractal and euclidean nonequilibrium growth patterns of ice i_h in supercooled water. *Dokl. Phys. Chem.*, 389:94–97, 2003.

[44] A. A. Shibkov, Y. I. Golovin, M. A. Zheltov, A. A. Korolev, and A. A. Leonov. Morphology diagram of nonequilibrium patterns of ice crystals growing in supercooled water. *Physica A*, 319:65–79, 2003.

[45] A. A. Shibkov, M. A. Zheltov, A. A. Korolev, A. A. Kazakov, and A. A. Leonov. Crossover from diffusion-limited to kinetics-limited growth of ice crystals. *Journal of crystal growth*, 285(1):215–227, 2005.

[46] L. Symons and A. Perry. Predicting road hazards caused by rain, freezing rain and wet surfaces and the role of weather radar. *Meteorological applications*, 4(1):17–21, 1997.

[47] K. Szilder, E. P. Lozowski, and G. Reuter. A Study of Ice Accretion Shape on Cables Under Freezing Rain Conditions. *J. Offshore Mech. Arct. Eng. Trans. ASME*, 2002.

[48] A. L. Yarin. Drop impact dynamics: splashing, spreading, receding, bouncing ... *Annu. Rev. Fluid Mech.*, 38:159–192, 2006.

[49] A. L. Yarin, I. V. Roisman, and C. Tropea. *Collision Phenomena in Liquids and Solids*. Cambridge University Press, 2017.

[50] A. L. Yarin and D. A. Weiss. Impact of drops on solid surfaces: self-similar capillary waves, and splashing as a new type of kinematic discontinuity. *Journal of Fluid Mechanics*, 283:141–173, 1995.

[51] W. P. Zakrzewski. Splashing a ship with collision-generated spray. *Cold Reg. Sci. Tech.*, 14(1):65–83, 1987.